Jpn. J. Appl. Phys. Vol. 36 (1997) pp. 4558–4562
Part 1, No. 7B, July 1997

Electron Heating and Control of RF-Produced Plasma Parameters Excited by a Planar, Spiral Antenna

Seiji TAKECHI*, Shunjiro SHINOHARA and Yoshinobu KAWAI
Interdisciplinary Graduate School of Engineering Sciences, Kyushu University, Kasuga, Fukuoka 816, Japan

(Received January 21, 1997; accepted for publication March 24, 1997)

Electron heating in inductively coupled plasma with use of a planar, spiral antenna is investigated by measurement of the skin depth of evanescent waves and antenna-plasma coupling. It is shown that for plasma production, both a collisionless and a collisional heating mechanism play an important role in a wide range of collision frequencies. In addition, control of plasma parameters such as uniformity and density by adjustment of the antenna configuration and the external magnetic field is demonstrated.

KEYWORDS: RF plasma, ICP, spiral antenna, evanescent wave, skin depth, antenna-plasma resistance, magnetic field, uniformity

1. Introduction

A helicon wave plasma[1–6] and inductively coupled plasma/transformer coupled plasma (ICP/TCP)[7] are expected to be used as high-density plasma sources required for, *e.g.*, plasma processing and confinement devices, and characteristics of these plasmas in the radio frequency (RF) range have been investigated in detail experimentally and theoretically. A planar, spiral coil[8–11] has been used in ICP due to the advantage of its simple geometry, but some problems remain to be solved, such as the antenna-plasma coupling and RF wave phenomena, in elucidation of RF-produced plasma characteristics.

As for antenna-plasma coupling, in some cases, capacitive (electrostatic) coupling is dominant at low RF power, whereas inductive (electromagnetic) coupling is dominant at high RF power after the density jump (a steep increase in density by the application of RF threshold power).[12] For checking of these two different discharge regions, studies on antenna-plasma coupling are important. Previously obtained experimental results indicate that inductive coupling is dominant in RF plasma discharge by this spiral antenna in a wide range of our experimental conditions such as RF power, Ar filling pressure and magnitude of uniform magnetic field.[10,11] In addition, the study on antenna-plasma coupling is useful for elucidation of the electron heating mechanism in ICP.[13,14] Here, experimentally observed plasma loading resistance (coupling) and skin depth of evanescent waves are compared with those obtained from collisional and collisionless models[10,13,15] for various collision frequencies.

With a static axial magnetic field, radial diffusion can be altered and, in contrast to the evanescent wave in the ICP case, a propagating wave can be expected to be excited in certain cases. In fact, when an external magnetic field was applied, the observed spatial profiles of plasma parameters changed, and the spatial profiles of excited magnetic fields and the dispersion relation showed that a helicon wave with a dominant azimuthal mode number of $m = 0$ could be excited.[10,11] These results mean that this external magnetic field can be expected to be an additional control parameter for the plasma discharge.

In this study, we concentrate on, in addition to investigating the electron heating process in ICP, the control of plasma parameters by changing the antenna field pattern and the external magnetic field configuration.

2. Experimental Setup

The experimental setup is the same as that shown in Fig. 1 of ref. 10. The four-turn, water-cooled, spiral antenna (without a Faraday shield) with a diameter of 18 cm is made of copper. In some cases, a disk shield, made of copper, which covers the inner two-turn portion of the spiral antenna, can be placed over the antenna in order to use the outer two-turn portion only. The distance between the surface of the antenna and the quartz

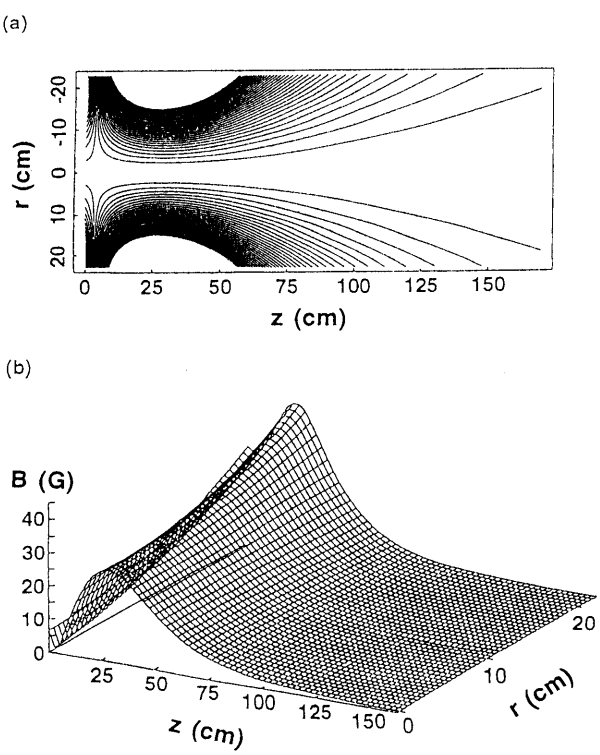

Fig. 1. (a) Contour plot of the magnetic flux. (b) Radial and axial profiles of the magnitude of the external magnetic field. Here, coil current I_c is 60 A and distance d between the two coils is 36 cm.

*E-mail address: scijiigh@mbox.nc.kyushu-u.ac.jp

window, which is 25 cm in diameter and 0.8 cm thick, is 1.7 cm. Here, $z = 0$ cm is defined as being at the window surface which faces an inner vacuum chamber $\sim$ 45 cm in diameter and $\sim$ 170 cm in length. In order to control the plasma parameters, an external magnetic field is applied which is generated mainly by two coils: currents with the same magnitude have opposite directions, and the position of one coil is fixed at $z = -14$ cm (the other coil is at $z > 0$ cm). A typical contour plot of magnetic flux (line cusp position $z_{\mathrm{cusp}} = 4$ cm, and the ratio R of this length to the observed maximum skin depth in ICP is ~ 2), and a two-dimensional profile of the magnitude of the magnetic field are shown in Figs. 1(a) and 1(b), respectively. Here, the central distance d between the two coils is 36 cm and coil current I_{c} is 60 A (each coil has 48 turns).

The RF power and frequency are < 2 kW and 7 MHz, respectively, and the RF output pulse has a width of 5 ms (duty of 1/8) under the condition of high RF power to protect against thermal damage. The RF power supply is connected to the antenna through a directional coupler, which picks up the incident and reflected power, P_{inc} and P_{ref}, respectively, a matching box and devices to monitor the antenna voltage and current between the antenna and matching box. Argon plasma parameters are measured by use of movable Langmuir and magnetic probes inserted into the plasma radially and axially.

3. Skin Depth and Plasma Resistance in ICP

Figures 2(a)–2(c) show typical axial profiles of measured B_z (axial component of the excited magnetic fields), n_{e} (electron density) and T_{e} (electron temperature) at the plasma center in ICP, respectively, for an input RF power P_{inp} $(= P_{\mathrm{inc}} - P_{\mathrm{ref}})$ of $\sim$ 360 W. Normally, B_z amplitude decreases exponentially in the z direction and the skin depth can be estimated from this slope. However, Fig. 2(a) shows that, at relatively lower pressure, B_z does not decrease monotonically. This field pattern is not predicted from cold plasma theory, but can be expected considering the effect of electron thermal motion.[16] The minimum point of the absolute value of B_z is considered to represent the optimum chamber length related to the resonant coupling between the field and the electron bounce motion from the effective boundaries in low collisionality. The resonance occurs when electrons travel the chamber length L in a time equal to a multiple of half the wave period; i.e., $(2/\pi) \times (\omega L/v_{\mathrm{th}})$ is an integer. Here, ω is the driving angular frequency, v_{th} is the electron thermal velocity, and the position of the minimum point is held constant even when the chamber length is sufficiently longer than the optimum length.[16] In our experiment, both conditions of $(2/\pi) \times (\omega L/v_{\mathrm{th}}) > 1$ and $(2/\pi) \times (\omega\delta/v_{\mathrm{th}}) < 1$ (condition of collisionless model[13,16] where δ is the skin depth) are satisfied. As far as we know, this is the first time that the field pattern has been observed experimentally by use of the asymmetric antenna configuration in the axial direction and a cylindrical chamber. In Figures 2(b) and 2(c), it is shown that n_{e} is almost constant and T_{e} decreases slightly as z increases, respectively.

Figure 3(a) shows the dependences of the measured

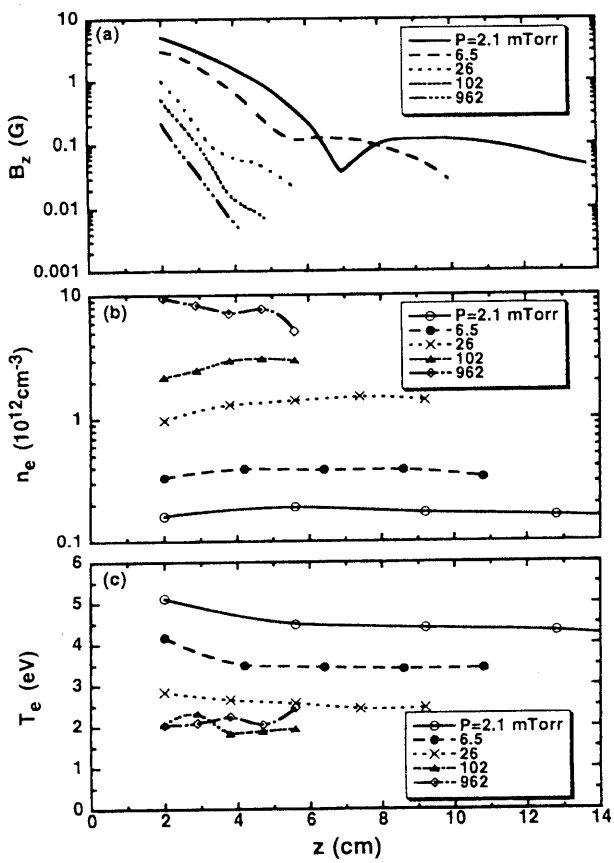

Fig. 2. Axial profiles of (a) the excited axial magnetic field B_z, (b) electron density n_{e} and (c) electron temperature T_{e} at the plasma center.

skin depth and this depth calculated from collisional[15] and collisionless[13] models, respectively, on the normalized collision frequency ν/ω, with changing the filling pressure (ν: sum of electron-neutral elastic and electron-ion Coulomb collision frequencies). Here, the ratio of the electron-ion Coulomb collision frequency to that of the electron-neutral elastic collision is 0.1–0.4 in the range of ν/ω less than $\sim$ 10, while it is less than 0.1 in the range of ν/ω greater than $\sim$ 10. Therefore, electron-neutral elastic collision is dominant throughout this experiment. For collisional[15] and collisionless[13] models, the skin depth corresponds to $\delta_{cl} = (c/\omega_{\mathrm{pe}})[2(1+\nu^{*2})/(1+(1+\nu^{*2})^{0.5})]^{0.5}$ and $\delta_{cs} = [(2eT_{\mathrm{e}}/\pi m_{\mathrm{e}})^{0.5}(c^2/\omega_{\mathrm{pe}}^2\omega)]^{(1/3)}$, respectively ($c$: velocity of light, ω_{pe}: electron-plasma angular frequency, e: elementary electric charge, m_{e}: electron mass, $\nu^* = \nu/\omega$, T_{e} in eV). These skin depth and plasma parameters are average ones for a region of $z = 2$–3.8 cm. The measured skin depth is considered to be nearly equal to the ideal skin depth with infinite plane geometry, since the skin depth in the absence of the plasma is $\sim$ 3.2 cm (from Fig. 1 in ref. 11), which corresponds to the decay length of the RF field limited by the boundaries and the antenna geometry. This result shows that measured skin depth roughly agrees to calculated depth, and is longer in the low ν/ω region and nearly constant in the high ν/ω region. Figure 3(b) shows the dependences of the measured plasma loading resistance R_{p} and calculated resistances from collisional and collisionless models in one dimension,[13] on ν/ω.

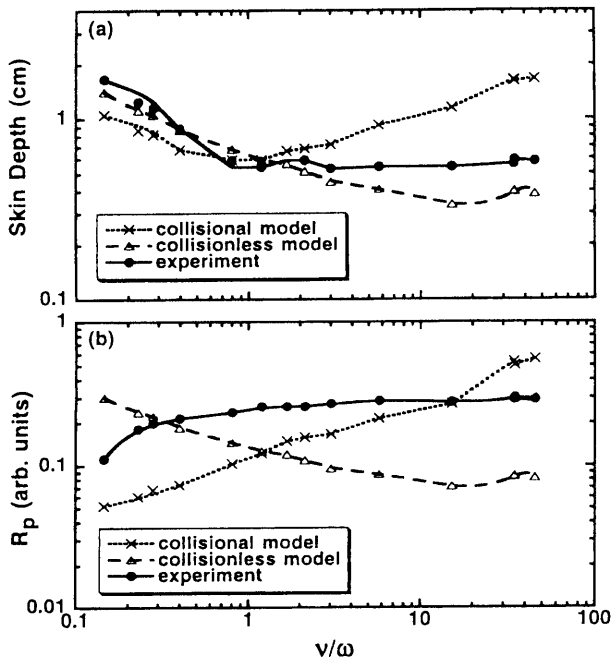

Fig. 3. (a) Dependences of experimentally obtained skin depth and skin depth calculated from collisional and collisionless models on normalized collision frequency ν/ω. (b) Dependences of experimentally obtained loading resistances R_p and calculated resistances from the two models on ν/ω.

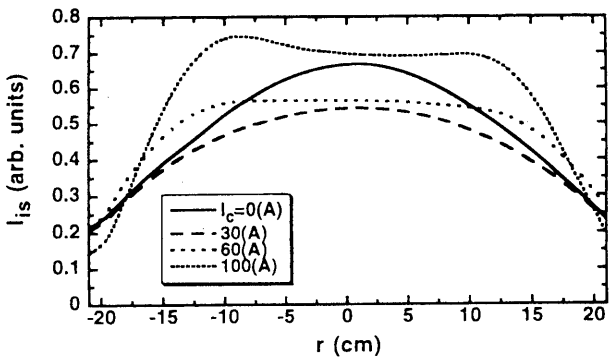

Fig. 4. Radial profiles of ion saturation current I_{is} at $z = 30$ cm, for various coil currents I_c. Here, filling pressure P is 8.5 mTorr and input RF power P_{inp} is ~ 300 W.

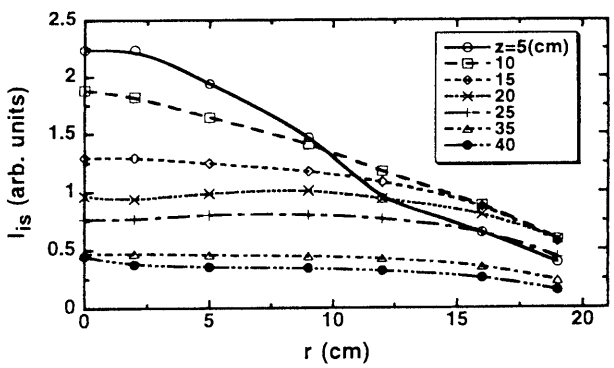

Fig. 5. Radial profiles of ion saturation current I_{is} for various axial positions. Here, filling pressure P is 8.5 mTorr, input RF power P_{inp} is ~ 300 W and coil current $I_c = 60$ A.

The measured R_p is $(P_{inp}/I^2) - R_0$ (I: effective current flowing in the antenna, R_0: the vacuum loading resistance). The R_p calculated from collisional and collisionless models[13] is the real part of the surface impedance, i.e., $[\nu^*/2(1+\nu^{*2})^{0.5}]\mu_0\omega\delta_{cl}$ and $(2/3^{1.5})\mu_0\omega\delta_{cs}$, respectively ($\mu_0$: permeability in a vacuum). This tendency shows that the observed R_p is weakly dependent on ν/ω, and the effect of the collisionless (collisional) heating on RF energy dissipation is suggested to occur in the lower (higher) ν/ω region. Therefore, both collisionless and collisional heating mechanisms can be expected to play an important role for plasma production in a wide range of ν/ω under our experimental conditions.

4. Control of Plasma Parameters

Figure 4 shows radial profiles of ion saturation current I_{is} at $z = 30$ cm for various coil currents I_c (the same magnetic field configuration as shown in Fig. 1(a)). Here, P_{inp} is ~ 300 W and P is 8.5 mTorr. As I_c, corresponding to the magnitude of the external magnetic field (*e.g.*, $I_c = 60$ A corresponds to 27 G at the center in the radial direction), is increased, the value of ion saturation current I_{is} at $r = 0$ cm is decreased and the radial profile becomes flatter. The effective diameter D_{eff} defined as the region where I_{is} is uniform within $\pm 5\%$ is ~ 27 cm at $I_c = 60$ A which is ~ 14 cm larger than that in the absence of the magnetic field. In addition, the radial profile of I_{is} at $I_c > 60$ A becomes hollow. Values of n_e and T_e at $I_c = 60$ A lie in ranges of 2.0–2.8×10^{11} cm^{-3} and 1.5–2.5 eV in a region of $r = -17$ cm–17 cm, respectively. Figure 5 shows radial profiles of ion saturation current I_{is} for various axial positions. Here, P is 8.5 mTorr and I_c is 60 A, and a relatively flatter profile of I_{is} in the region of $z = 20$–35 cm is observed.

Figures 6(a) and 6(b) show the dependences of ion saturation current I_{is} at $r = 0$ cm and D_{eff} derived from the radial profile of ion saturation current I_{is} at $z = 30$ cm, respectively, on coil current I_c (the same magnetic field configuration as shown in Fig. 1(a)). Here, the input RF power P_{inp} is ~ 300 W, and the filling pressures P are 1.3 and 8.5 mTorr. Figure 6(a) shows that the value of I_{is} at the plasma center for $P = 8.5$ mTorr decreases as I_c increases, and then begins to increase when I_c is greater than 40 A, in contrast to the case of $P = 1.3$ mTorr where the minimum point of I_{is} is observed at $I_c \sim 5$ A. Figure 6(b) shows that while D_{eff} at $P = 8.5$ mTorr increases as I_c increases and decreases slightly when I_c is greater than 60 A, D_{eff} at 1.3 mTorr decreases monotonically as I_c increases. These results are considered to be due to the dependence on the location of the observation region (axial position), in which the profile is governed by diffusion depending on the pressure (and plasma parameters) and/or the characteristics of the propagating wave.

Figure 7 shows radial profiles of ion saturation current I_{is} at $z = 30$ cm in the presence and absence of the magnetic field ($I_c = 45$ A), for two different antenna configurations: RF plasma is produced by a four-turn spiral antenna, or by the outer two-turn spiral antenna (a disk shield is placed over the four-turn spiral antenna). Here, P_{inp} is increased to ~ 1.5 kW (pulse discharge) and P is 8.5 mTorr. In the case of this outer two-turn antenna

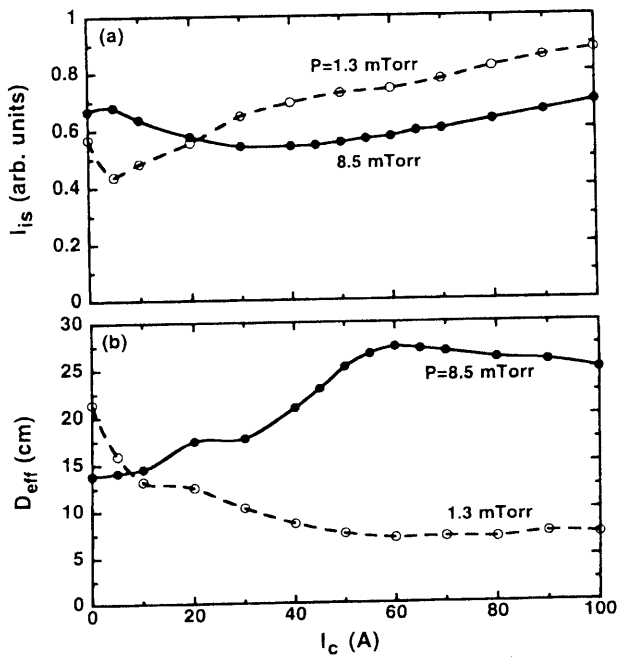

Fig. 6. Dependences of (a) ion saturation current I_{is} at the plasma center and (b) effective diameter D_{eff} on coil current I_c at $z = 30$ cm. Here, filling pressure P is 1.3 and 8.5 mTorr, and input RF power P_{inp} is ~ 300 W.

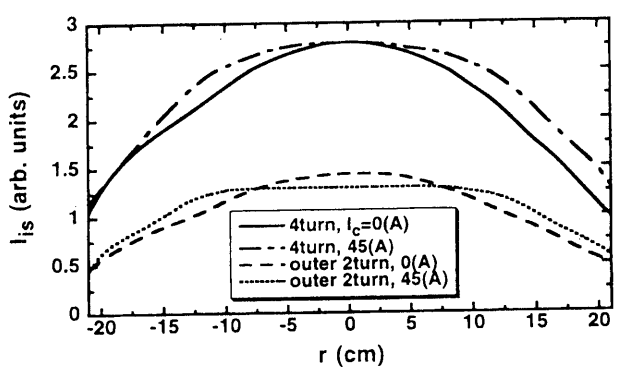

Fig. 7. Radial profiles of ion saturation current I_{is} at $z = 30$ cm in the presence (coil current $I_c = 45$ A) and absence of the magnetic field in the cases of the four-turn antenna and the two-turn antenna. Here, filling pressure P is 8.5 mTorr and input RF power P_{inp} is ~ 1.5 kW.

configuration, I_{is} at $r = 0$ cm and $I_c = 45$ A is ~ 2.3 times smaller than in the case of the four-turn antenna under the same conditions, but D_{eff} increases to ~ 27 cm (~ 3 cm larger than in the case of the four-turn antenna). Here, n_e and T_e at $I_c = 45$ A for the four-turn (outer two-turn) antenna lie in ranges of 0.9–1.3×10^{12} cm^{-3} (5.0–6.0×10^{11} cm^{-3}), and 1.3–2.5 eV (1.3–2.4 eV) within a region of $r = -17$ cm–17 cm, respectively. The D_{eff} up to ~ 27 cm, obtained using the outer two-turn antenna, is comparable to that in Fig. 4 (although the RF power is different). It is suggested that in the case of the outer two-turn antenna, the radial profile of I_{is} at $z = 30$ cm becomes flatter with decreasing magnetic field. This result indicates a significant relationship between the plasma parameters and the propagating region of a traveling wave and/or antenna near field changed by the

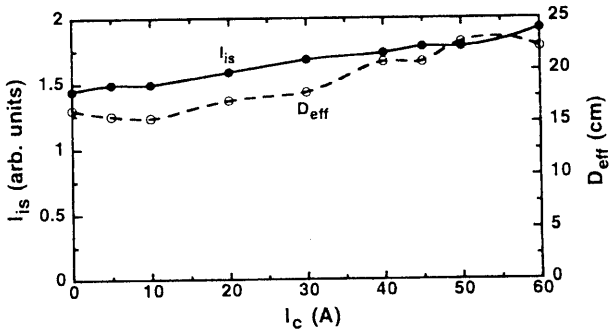

Fig. 8. Dependences of ion saturation current I_{is} at the plasma center and effective diameter D_{eff} obtained using the outer two-turn antenna at $z = 30$ cm. Here, filling pressure P is 8.5 mTorr, input RF power P_{inp} is ~ 1.5 kW and distance d between the two coils is 53 cm.

antenna configurations.

The radial profile of I_{is} at $z = 30$ cm is measured using the outer two-turn antenna, at $P = 8.5$ mTorr and $P_{inp} = \sim 1.5$ kW, and for various I_c and magnetic configurations: 1) in the presence of uniform magnetic field ($B < 72$ G); 2) in the presence of only one magnetic field coil at $z = -14$ cm and $I_c < 20$ A corresponding to 4.6 G at the plasma center with $z = 30$ cm; 3) in the presence of two coils at $I_c < 10$ A corresponding to 0.5 G at the center and $d = 84$ cm, line cusp position $z_{cusp} = 28$ cm and a ratio R of z_{cusp} to the observed maximum skin depth in ICP of ~ 14; 4) in the presence of two coils at $I_c < 60$ A corresponding to 27 G at the center and $d = 53$ cm, $z_{cusp} = 12.5$ cm and $R \sim 6$; and 5) in the presence of two coils at $I_c < 100$ A corresponding to 40 G at the center and $d = 31$ cm, $z_{cusp} = 1.5$ cm and $R \sim 0.5$. In the case of 1), 2) and 3), the radial profile of ion saturation current I_{is} is more peaked and the value at the center is larger than that in the absence of the magnetic field (for the same magnetic configuration as in the case of 1), more detailed results in the presence and absence of a Faraday shield are presented in refs. 10 and 11). In contrast, in the cases of 4) and 5), the dependence of D_{eff} on I_c is similar to that when d is 36 cm (but the maximum value of $D_{eff} \sim 23$ cm is smaller than that in Fig. 7 and I_{is} at $r = 0$ cm gradually increases, as shown in Fig. 8 for the case of 4), and the plasma discharge cannot be maintained at I_c greater than 60 A). The above results show that D_{eff} cannot be improved by the use of uniform and divergent magnetic fields as compared to one in the absence of the applied magnetic field, and the relationship between the location of the observation region and the position of the line cusp in the cusp magnetic field configuration is important for obtaining larger D_{eff}.

In summary, in this experiment, the maximum value of D_{eff} reached ~ 27 cm (increased by more than 10 cm over the value obtained in a previous experiment under the same experimental conditions) as a result of changing the antenna field pattern and the external magnetic field configuration.

5. Conclusions

The electron heating mechanism in inductively coupled plasma with use of a planar, spiral antenna is in-

vestigated experimentally. The axial profile pattern of the evanescent wave amplitude is measured, and the experimentally observed skin depth of this evanescent wave and plasma loading resistance are compared with those calculated from collisional and collisionless models, for various filling pressures. These results suggest the dominance of the collisionless (collisional) heating mechanism in lower (higher) collisionality from the data in a wide range of collision frequency.

Successful control of plasma parameters by changing the antenna field pattern and external magnetic field configuration (cusp field) has been demonstrated. It is shown that the effective diameter D_{eff}, at which $z = 30\,\mathrm{cm}$, $P = 8.5\,\mathrm{mTorr}$ and $d = 36\,\mathrm{cm}$, increases to $\sim 27\,\mathrm{cm}$, with both the four-turn spiral antenna ($P_{\mathrm{inp}} \sim 300\,\mathrm{W}$ and $I_{\mathrm{c}} = 60\,\mathrm{A}$) and the outer two-turn antenna ($P_{\mathrm{inp}} \sim 1.5\,\mathrm{kW}$ and $I_{\mathrm{c}} = 45\,\mathrm{A}$).

We are investigating the excited wave characteristics, from the viewpoint of a propagating wave, in order to elucidate the physical mechanism underlying the observed phenomena, and more detailed results will be presented later.

1) R. W. Boswell: Plasma Phys. Control. Fusion **26** (1984) 1147.
2) F. F. Chen: Plasma Phys. Control. Fusion **33** (1991) 339.
3) A. Komori, T. Shoji, K. Miyamoto, J. Kawai and Y. Kawai: Phys. Fluids **B3** (1991) 893.
4) T. Shoji, Y. Sakawa, S. Nakazawa, K. Kadota and T. Sato: Plasma Sources Sci. Technol. **2** (1993) 5.
5) S. Shinohara, Y. Miyauchi and Y. Kawai: Plasma Phys. Control. Fusion **37** (1995) 1015.
6) S. Shinohara and Y. Kawai: Jpn. J. Appl. Phys. **34** (1995) L1571.
7) J. Hopwood: Plasma Sources Sci. Technol. **1** (1992) 109.
8) J. Hopwood, C. R. Guarnieri, S. J. Whitehair and J. J. Cuomo: J. Vac. Sci. Technol. **A II** (1993) 147.
9) J. A. O'Neil, M. S. Barnes and J. H. Keller: Appl. Phys. Lett. **73** (1993) 1621.
10) S. Shinohara, S. Takechi and Y. Kawai: Jpn. J. Appl. Phys. **35** (1996) 4503.
11) S. Takechi, S. Shinohara and Y. Kawai: *Proc. Int. Conf. on Plasma Phys.* (Nagoya, 1996) 10A17.
12) J. Amorim, H. S. Maciel and J. P. Sudano: J. Vac. Sci. Technol. **B9** (1991) 363.
13) M. M. Turner: Phys. Rev. Lett. **71** (1993) 1844.
14) V. A. Godyak, R. B. Piejak and B. M. Alexandrovich: Plasma Sources Sci. Technol. **3** (1994) 169.
15) S. Shinohara and Y. Kawai: Jpn. J. Appl. Phys. **35** (1996) L725.
16) N. S. Yoon, S. S. Kim, C. S. Chang and Duk-In Choi: Phys. Rev. E **54** (1996) 757.